41st AIAA/ASME/SAE/ASEE Joint Propulsion Conference & Exhibit
Tucson Convention Center, Tucson, Arizona
July 10–13, 2005

AIAA-2005-3797

Flight Research of an Aerospike Nozzle Using High Power Solid Rockets

Trong T. Bui* and James E. Murray†
NASA Dryden Flight Research Center, Edwards, CA, 93523

Charles E. Rogers‡
Air Force Flight Test Center, Edwards Air Force Base, CA, 93523

Scott Bartel§
blacksky Corporation, Carlsbad, CA, 92008

and

Anthony Cesaroni** and Mike Dennett††
Cesaroni Technology/Cesaroni Aerospace, Sarasota, FL, 34243

Flight research has been conducted on an aerospike rocket nozzle using high power solid rockets. Two aerospike rockets and one conventional rocket were flown successfully to supersonic speeds, providing the first known set of transonic flight performance data for aerospike rockets. This paper describes the rockets, solid rocket motors, nozzles, and rocket instrumentation system. Flight test results are also discussed and compared with ground test results. Flight data show that all of the rockets successfully reached supersonic speeds with a maximum Mach number of 1.6 and a peak pressure altitude of nearly 30,000 ft. The aerospike nozzle efficiency was determined to be 0.96 from computational fluid dynamics (CFD) analysis. The rocket chamber pressures and thrusts of the aerospike rocket motors were lower than the conventional rocket motors. Because the same propellant formulation was used in all of the rocket motors, the discrepancy in pressure and thrust was most likely caused by a larger actual aerospike nozzle throat area than the designed throat area. Potential causes for the larger aerospike nozzle throat area are also discussed.

Nomenclature

A_e	=	nozzle exit area
A_{ref}	=	rocket airframe cross-sectional area
A_t	=	nozzle throat area
A_x	=	measurement from the axial accelerometer
a_x	=	axial acceleration
C_d	=	rocket drag coefficient
C_T	=	nozzle coefficient of thrust
$C_{T,\ actual}$	=	actual nozzle coefficient of thrust
$C_{T,\ ideal}$	=	ideal nozzle coefficient of thrust
CFD	=	computational fluid dynamics

* Aerospace Engineer, Propulsion and Performance, MS 2708, PO Box 273, AIAA Senior Member.
† Aerospace Engineer, Research Aerodynamics, MS 2228, PO Box 273.
‡ Lead Engineer, Hypersonic Flight Test Team, 412th Test Wing/DRP(HFTT).
§ President, 5674 El Camino Real, Suite H, AIAA Senior Member.
** President/CEO, 1144 Tallevast Road.
†† Lead Engineer, Propulsion, 1144 Tallevast Road.

d = diameter
D = external aerodynamic drag of the rocket
FADS = flush air data system
F_x = forces in the axial direction
g = gravitational acceleration
ISP = specific impulse
M = Mach number
m = rocket mass
$\dot{m}$ = rocket propellant mass flow rate
P_a = ambient pressure
P_c = rocket chamber pressure
psig = pounds per square inch gage
r = radius
T = rocket motor thrust
t = time
u_x = rocket velocity in the axial direction
U_∞ = freestream velocity
x = axial direction
γ = specific heat ratio
η_t = nozzle efficiency factor
ρ_∞ = freestream density
θ = rocket elevation angle

I. Introduction

THE broad range of human and robotic space exploration missions to the Moon, Mars, and destinations beyond, as outlined in the President's Space Exploration Vision, will benefit from advances in technology from all systems of a space vehicle, including the propulsion system and its nozzle. Most space vehicles, including space-launch boosters, Moon and Mars landers, orbiters, space tugs, or deep-space interplanetary probes, rely on a nozzle to convert the energy generated in the propulsion system into the direct thrust necessary to propel them through space. This is true for chemical, nuclear thermal, solar-heating, and arc-heating rockets. Therefore, nozzle efficiency and its physical size have a primary effect on the overall performance of space vehicles. Increased nozzle efficiencies and shorter nozzle lengths translate directly into less weight, more payload, longer range, and lower costs across the entire spectrum of space vehicles.

Reference 1 provides a broad review of advanced rocket nozzle technologies. In this reference, it is shown that altitude-compensating nozzle technologies, such as the expansion-deflection nozzle, aerospike or plug nozzle, dual-bell nozzle, and dual-expander nozzle, can provide significant performance gains by adapting the nozzle exhaust flow to changes in ambient pressure.

One of the promising altitude-compensating nozzle technologies that has received considerable attention from the aerospace research community is the aerospike nozzle. A good discussion on the aerospike nozzle flow physics can be found in reference 2. For solid rocket motors, an aerospike nozzle was designed, built, and ground tested by Johnson and Leary.[3] Besnard, Chen, Mueller, and Garvey[4] designed, fabricated, and ground tested an aerospike nozzle for liquid rocket engines as part of the California Launch Vehicle Education Initiative (CALVEIN). The CALVEIN aerospike effort eventually resulted in the first known flight of a liquid-fueled aerospike rocket in December 2003.

In addition to the altitude-compensation ability, aerospike nozzles can provide more thrust in the vacuum of space or on the Moon. Compared to the 50:1 ratio nozzles used on the Apollo Lunar Excursion Module descent and ascent stages, as well as the Apollo Service Module, aerospike rocket nozzles with expansion ratios of 200:1 to 300:1 would increase thrust and specific impulse by 5 to 6 percent. For the high Delta-V demands of orbital transfer systems, as well as the descent and ascent stages for missions to the Moon and Mars, a 5 to 6 percent increase in specific impulse could result in an approximate 8 to 9 percent decrease in propellant mass. This significant mass savings lowers the total vehicle mass for a Moon or Mars mission and provides margin for other critical vehicle systems or payloads. Truncated aerospike nozzles also have the advantage of being more compact than conventional bell nozzles for in-space applications.

In addition to space exploration applications, the aerospike nozzles can offer advantages in defense applications such as air-to-air, ground-to-ground, and ground-to-air missile systems. Many current tactical missile systems have

fixed, non-adaptive nozzles. Yet even air-to-air missiles might be launched from a wide range of altitudes against targets at yet different altitudes. Also each missile trajectory might cover a wide range of altitudes during normal operation. Altitude-compensating nozzles such as the aerospike nozzles might increase the performance of a missile system without the mechanical complexity of the conventional variable nozzles.

Although the advantages of altitude-compensating rocket nozzle technologies are well known through analysis and ground testing, the lack of actual atmospheric flight research data has hindered the use of these nozzles in current as well as a next generation of space vehicles. A comprehensive flight test data base, and preferably, actual rocket flights with altitude-compensating nozzles, such as the aerospike nozzles, are necessary before these nozzles can be seriously considered for actual application on space vehicles.

The current effort addresses the lack of atmospheric flight research data on altitude-compensating rocket nozzles by conducting transonic flight research and demonstration of an aerospike rocket nozzle using high power solid-fueled rockets within the atmosphere. The research approach is described in this paper. Results from analysis, ground tests, and actual rocket flight tests are presented and discussed.

Trade names and trademarks are used in this report for identification only. Their usage does not constitute an official endorsement either expressed or implied, by the National Aeronautics and Space Administration.

II. Research Approach

Rapid progress in aerospace technologies requires a constant interplay between analysis, ground testing, and flight testing activities. All three of these activities are equally important. Testing, both on the ground and in flight, keeps analysis well-grounded and relevant, while analysis provides the foundation and explains flight and ground test results. Often, the sparks of insight gleaned from one of these activities greatly benefits the other two, if all three activities are done in concert, accelerating the maturation of advanced aerospace technologies.

Figure 1 summarizes the approach of the current research effort. During a two-year period and with a small discretionary budget, a comprehensive effort was undertaken with analysis, ground testing, as well as flight-testing, all conducted in a complementary and integrated manner. In this project, an aerospike solid-fueled rocket nozzle was designed, built, ground tested, and flight tested. This aerospike nozzle was successfully used to power two solid-fueled rockets to supersonic flight speeds on two consecutive flights, providing the first known set of transonic flight performance data for aerospike rockets. A conventional conical nozzle rocket with an identical configuration was also flown to supersonic speeds, providing valuable baseline comparison data. Key to this effort is a cost-effective, high-speed flight research rocket vehicle utilizing consumer-grade high power rocketry techniques, procedures, and materials. Also, resources and personnel from the high power rocketry organizations such as the Tripoli Rocketry Association (Orem, UT) were critical to the success of this project. Hopefully this new flight research vehicle will allow new propulsion concepts and small research payloads to take flight quickly and frequently, helping to bridge the gap that currently exists between analysis, ground testing, and flight for advanced aerospace technologies.

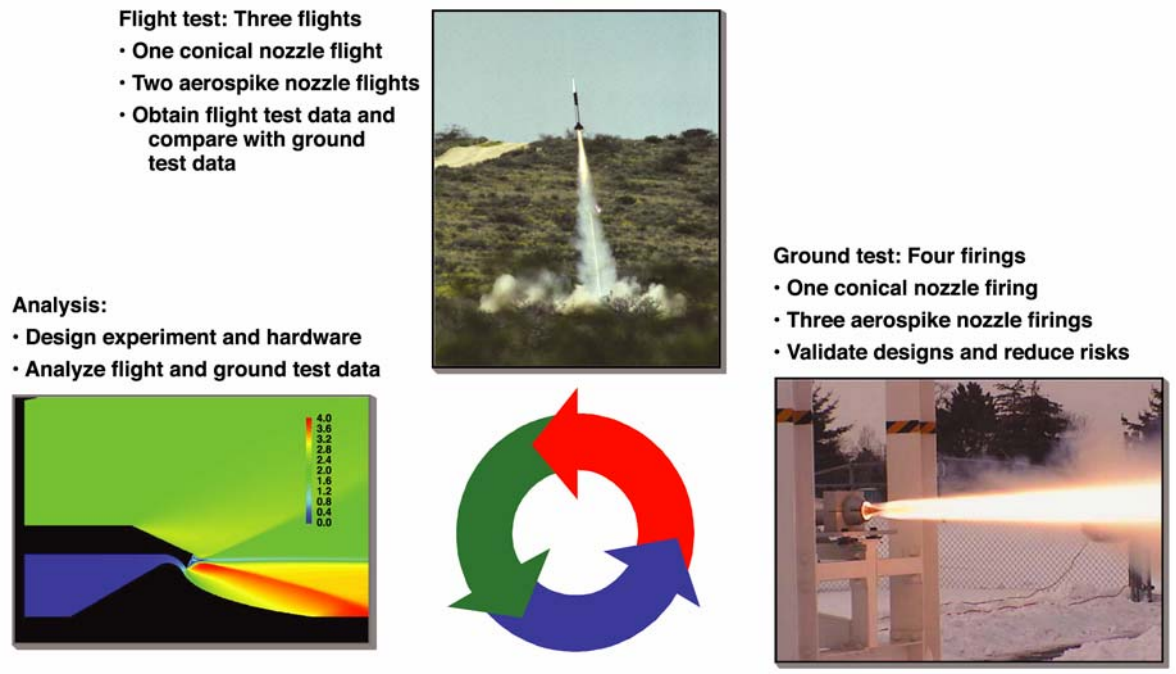

Figure 1. Current Research Effort Includes Analysis, Ground Testing, and Flight Testing.

A. Rocket Test Vehicle

The Optimal 168 rocket from blacksky Corporation (Carlsbad, CA) was used as the primary rocket test vehicle for this flight research effort. Engineering drawings of the Optimal 168 rocket are shown in figure 2 below, both with the aerospike rocket nozzle as well as the conventional conical nozzle. The total lift-off weight of the rocket test vehicle is just under 100 lb. The aerospike rocket is 125.32 in. long from the virtual rocket nose cone tip to the end of the aerospike nozzle plug. The conventional rocket is 120.70 in. long. The rocket airframe is a single piece of extruded 6061 aluminum tube with a nominal outer diameter of 6.63 inches. The fiberglass nose cone is a simple cone with a total conical angle of 10 deg. This nose cone geometry was chosen because an extensive aerodynamic database is available for this simple geometric shape. The rocket nose cone has a stainless steel nose tip which houses a total pressure port with a port inlet diameter of 0.125 in. A simple Flush Air Data System (FADS)[5], consisting of a set of four wall static pressure ports on the nose cone, is used to determine the incoming freestream flow angle. The FADS pressure ports are located 26.62 in. from the virtual nose tip and distributed circumferentially around the nose cone at equal 90-deg intervals. One wall static pressure port is also located on the rocket airframe at 66.54 in. from the virtual nose tip. The nose cone total pressure port and static pressure ports, as well as the airframe static pressure port, provide the air data measurements necessary to determine the rocket flight Mach number, pressure altitude, and incoming freestream flow angles. To minimize lags in pressure measurements, all of the nose cone pressure transducers are mounted within the nose cone itself. Two other pressure transducers are mounted inside the rocket airframe: the rocket chamber gage pressure transducer and the internal reference pressure transducer, used to provide the reference pressure for the rocket chamber gage pressure measurement.

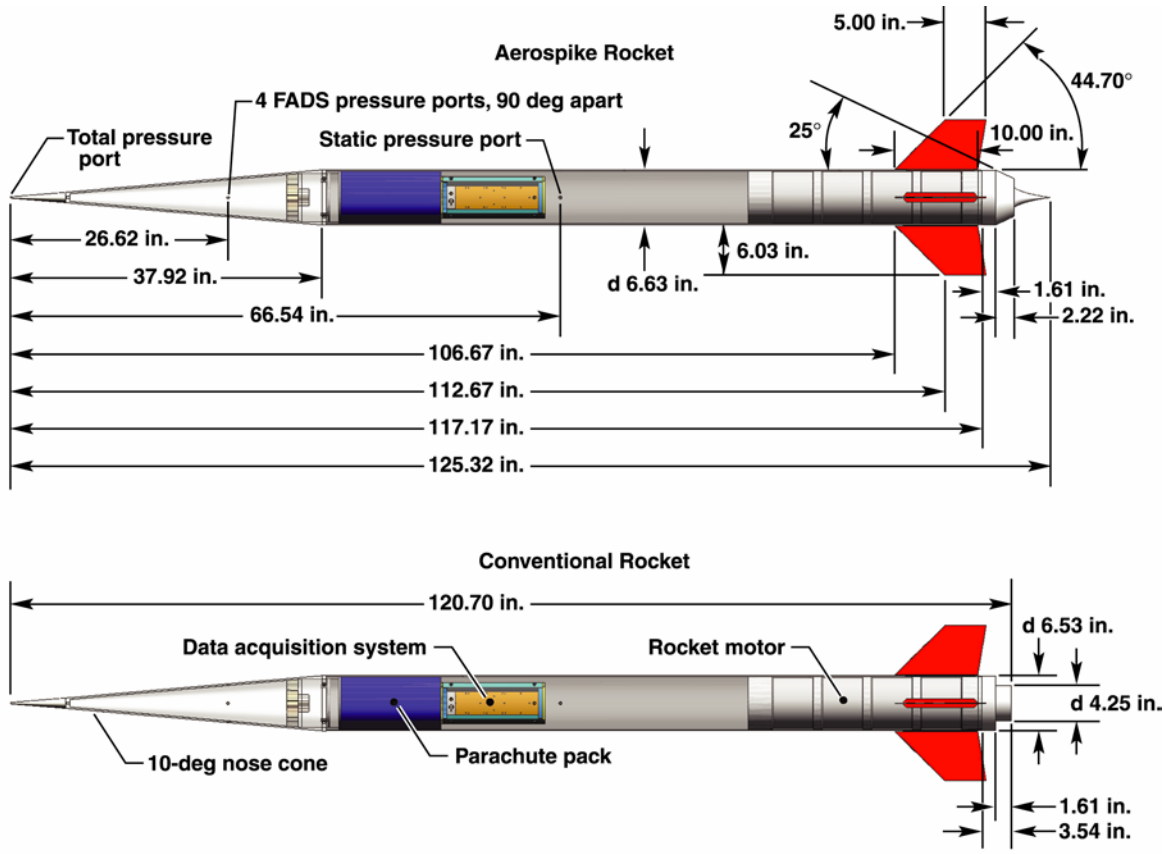

Figure 2. Engineering Drawings of the Aerospike Rocket and the Conventional Rocket Used in the Dryden Aerospike Rocket Test.

The rocket recovery system is located directly below the nose cone, consisting of the parachute system, two blacksky AltAcc altimeter and accelerometer data acquisition and recovery controllers, and an Advanced Retention and Release Device (ARRD) – a pyrotechnic release device for the main chute. The parachute pack has one 5-ft diameter drogue chute and one 12-ft diameter main chute. Actuated by the dual-redundant AltAcc onboard controllers, the drogue chute deploys at minimum rocket velocity (apogee). Then the main chute deploys when the rocket descends to approximately 2500 ft above ground level and the ARRD is fired. Two VHF homing beacon radio transmitters with different manufacturers and frequencies are secured to the rocket chute harnesses to aid in locating the rocket after it lands. The rocket flight data acquisition system is mounted inside the rocket airframe directly below the rocket recovery package. The four rocket fins are formed from sheets of 5053 aluminum alloy and anodized red. From analysis, it was determined that the center-of-pressure (CP) of the rocket is always at least two rocket diameters behind its center of gravity (CG), ensuring stable flight throughout the rocket trajectory.

The vast majority of the rocket systems, including the rocket hardware, flight data acquisition electronics, sensors, recovery system, and recovery electronics are commercially available and thus are low-cost, low-risk items. The aerospike nozzle is the only “new” and high-risk item in this research effort. The chance for success in a flight research project greatly increases if the number of “new” and high-risk items is kept to the minimum (only one in this effort).

B. Solid Rocket Motor

The solid rocket motor used in this effort was developed by Cesaroni Technology Incorporated (CTI, Sarasota, FL), from the CTI Pro150® O5100 consumer high power rocketry motor. This solid rocket motor has an interchangeable nozzle assembly so that the same rocket motor can be used with the aerospike nozzle as well as the conventional conical nozzle. The Pro150 motor was originally developed as the prototype solid-fueled booster for the U.S. Navy Affordable Weapons Program, in which the Pro150 motor was used to launch a small turbojet-powered cruise missile. The Pro150 motor has a reusable 6061 aluminum alloy case and uses ammonium perchlorate composite propellant (APCP). The current propellant has less aluminum metal content than the standard Pro150 motor to minimize solid-gaseous multiphase flow in the aerospike nozzle. The propellant weight for all motors used in the current effort is 28.53±0.09 lb per motor.

C. Rocket Instrumentation System

The custom-made onboard rocket instrumentation system is based on the Tattletale® Model 8 data logger (Onset Computer, Bourne, MA) integrated with the CF-8 compact flash nonvolatile memory module (Persistor Instruments, Bourne, MA). NASA Dryden-designed power supply and signal conditioning boards provide regulated excitation, gain, offset, and low-pass anti-aliasing filtering for each sensor channel. Dual-redundant rechargeable lithium battery packs provide all required power.

The entire rocket sensor suite consists of 14 transducers in 15 data acquisition channels. Table 1 provides information on the transducers used in the current research effort. Three orthogonal microelectromechanical systems (MEMS) accelerometers and three orthogonal MEMS rate gyros measure body-axis accelerations and angular rates, respectively. The rocket motor chamber pressure is measured by a stainless-steel 1000-psig pressure transducer screwed into a one-quarter-inch National Pipe Thread (NPT) in the forward bulkhead of the rocket motor casing. Two data acquisition channels are used to record the rocket chamber pressure: one coarse-resolution and one fine-resolution channel. The coarse-resolution channel has the wider measurement range, to capture any large transients in rocket chamber pressure; while the fine-resolution channel provides a high resolution measurement at a smaller range. A 30-psia pressure transducer inside the rocket airframe provides the reference pressure for the rocket motor chamber pressure gage measurement. The rocket airframe freestream static pressure is measured by a 30-psia pressure transducer plumbed to a flush static port on the side of the cylindrical rocket airframe. Rocket nose cone total pressure is measured with a 100-psia pressure transducer plumbed to the pitot port at the tip of the nose cone. Four 30-psia pressure transducers are plumbed to the rocket FADS nose cone pressure ports. To minimize the lag time in pressure measurements, each of the pressure transducers is installed near the corresponding measurement location. With the exception of the rocket motor chamber pressure transducer, each pressure transducer is mounted with the acceleration-sensitive axis normal to the rocket flight direction.

Table 1. Instrumentation List for the Dryden Aerospike Rocket Test

Parameter ID	Measurement	Manufacturer	Model	Range	Resolution	Accuracy
pt	Nose cone total pressure	Honeywell*	ASCX100AN	0-100 psia	0.024 psia	±0.5 psia
psc1	FADS 1 pressure		ASCX30AN	0-30 psia	0.007 psia	±0.15 psia
psc2	FADS 2 pressure		ASCX30AN	0-30 psia	0.007 psia	±0.15 psia
psc3	FADS 3 pressure		ASCX30AN	0-30 psia	0.007 psia	±0.15 psia
psc4	FADS 4 pressure		ASCX30AN	0-30 psia	0.007 psia	±0.15 psia
psl	Airframe static pressure		ASCX30AN	0-30 psia	0.007 psia	±0.15 psia
pmr	Motor reference pressure		ASCX30AN	0-30 psia	0.007 psia	±0.15 psia
pmf	Motor pressure (fine)	Measurement Specialties, Inc.**	MSP-600-01K-P-3-N-1	0-700 psig	0.17 psig	±2.5 psig
pmc	Motor pressure (coarse)		MSP-600-01K-P-3-N-1	0-1000 psig	0.24 psig	±2.5 psig
A_x	Axial acceleration	Analog Devices Inc.***	ADXL250JQC	±25 g	0.012 g	±0.05 g
A_y	Lateral acceleration		ADXL105JQC	±5 g	0.0024 g	±0.01 g
A_z	Transverse acceleration		ADXL105JQC	±5 g	0.0024 g	±0.01 g
p	Roll rate		ADXRS150EB	±150 deg/s	0.07 deg/s	±0.15 deg/s
q	Pitch rate		ADXRS150EB	±150 deg/s	0.07 deg/s	±0.15 deg/s
r	Yaw rate		ADXRS150EB	±150 deg/s	0.07 deg/s	±0.15 deg/s

* Freeport, Illinois
** Hampton, Virginia
*** Norwood, Massachusetts

The data logger is programmed in C to sample the 15 data channels at 200 samples per second and at a 12-bit resolution. The samples are double-buffered in RAM onboard the data logger and copied to the nonvolatile compact flash memory at 1.28-second intervals. Data logging is started manually prior to launch and continued throughout flight and parachute descent. Data logging is also terminated manually after the rocket is recovered. The onboard recorded data are then transferred to a laptop PC via a high-speed serial link for postflight processing. For a faster data transfer, the flight data in the compact flash memory card can be transferred directly to a laptop PC using a compact flash USB card reader.

The flight data acquisition system and the battery packs are mounted inside a custom-built aluminum alloy "cage" for integration with the rocket. The integrated "cage" assembly with the flight data acquisition system was environmentally qualified for the rocket flight environment through a series of thermal, pressure, and vibration tests prior to the rocket launches. The flight data acquisition system performed well during environmental ground tests and all three rocket flights.

III. Analysis and Design

A. Nozzle Efficiency Analysis

The rocket nozzle efficiency, η_t, is defined as the ratio of the actual nozzle thrust coefficient divided by the ideal thrust coefficient, or

$$\eta_t = \frac{C_{T,actual}}{C_{T,ideal}} \tag{1}$$

From isentropic flow theory, the ideal thrust coefficient is

$$C_{T,ideal} = \sqrt{\frac{2\gamma^2}{(\gamma-1)}\left(\frac{2}{\gamma+1}\right)^{\frac{\gamma+1}{\gamma-1}}\left[1-\left(\frac{P_a}{P_c}\right)^{\frac{\gamma-1}{\gamma}}\right]} \tag{2}$$

This is the maximum possible thrust coefficient delivered by an ideal nozzle with no losses and perfect flow expansion at the nozzle exit.

The actual nozzle thrust coefficient is

$$C_{T,actual} = \frac{T}{P_c A_t} \tag{3}$$

The rocket motor thrust, T, is measured directly by a force balance during static rocket ground firings. In-flight rocket thrust is computed from flight data. Assuming that the rocket thrust acts in the same direction as the rocket flight direction, figure 3 shows a simple force diagram of a rocket in powered flight.

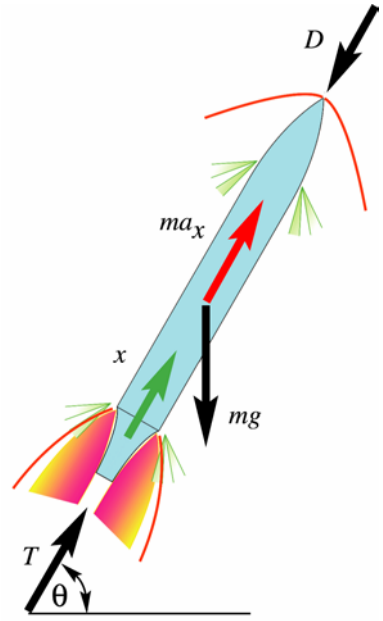

Figure 3. Simple Force Diagram From the Powered Rocket Flight.

Summation of the forces along the rocket flight direction (x-direction) gives

$$\sum F_x = d(mu_x)/dt \tag{4}$$

$$T - D - mg\sin(\theta) - ma_x = 0 \tag{5}$$

$$T - D - m\left(g\sin(\theta) + a_x\right) = 0 \tag{6}$$

Since

$$D = \frac{1}{2}\rho_\infty U_\infty^2 C_d A_{ref} \tag{7}$$

$$D = \frac{1}{2}\left(\gamma P_\infty M_\infty^2\right) C_d A_{ref} \tag{8}$$

and defining the quantity A_x, the actual measurement of the rocket axial accelerometer, as

$$A_x \equiv g\sin(\theta) + a_x \tag{9}$$

Solving equation (3) for thrust T, we have

$$T = \frac{1}{2}\left(\gamma P_\infty M_\infty^2\right) C_d A_{ref} + \left(m_{init} - \dot{m}\Delta t\right) A_x \tag{10}$$

The in-flight rocket thrust is thus a function of P_∞, M_∞, C_d, $\dot{m}$, and A_x. For rockets, there is a difference between the power-on C_d (rocket motor thrusting) and the power-off C_d (coasting). While the rocket motor is operating, the rocket plume pressurizes the rocket base region, reducing the rocket base drag. Since the rocket power-on C_d is presently not available, the rocket power-off C_d is used in equation (7).

B. Aerospike Nozzle Design

The aerospike nozzle uses a centered Prandtl-Meyer all-external expansion design. The geometrical shape for the central plug was obtained using a NASA Marshall Space Flight Center FORTRAN aerospike nozzle design code found in reference 6. Table 2 lists the design parameters for the aerospike rocket nozzle. To facilitate a direct comparison with the existing CTI conventional conical nozzle, the aerospike nozzle flow path has the same throat area and exit area as the conventional conical nozzle. The resulting aerospike nozzle flow path is shown in figure 4.

Table 2. Design Parameters for the Current Aerospike Rocket Nozzle

Design Parameters	Values
Throat area, A_t	1.853 in^2
Exit area, A_e	9.621 in^2
Exit area ratio, A_e/A_t	5.192
Rocket flow specific heat ratio, γ	1.194
Nozzle exit Mach number	2.802
Rocket chamber pressure	500 psia
Nozzle exit pressure	15.34 psia
Rocket flow specific gas constant	63.88 ft·lbf/(lbm·R)

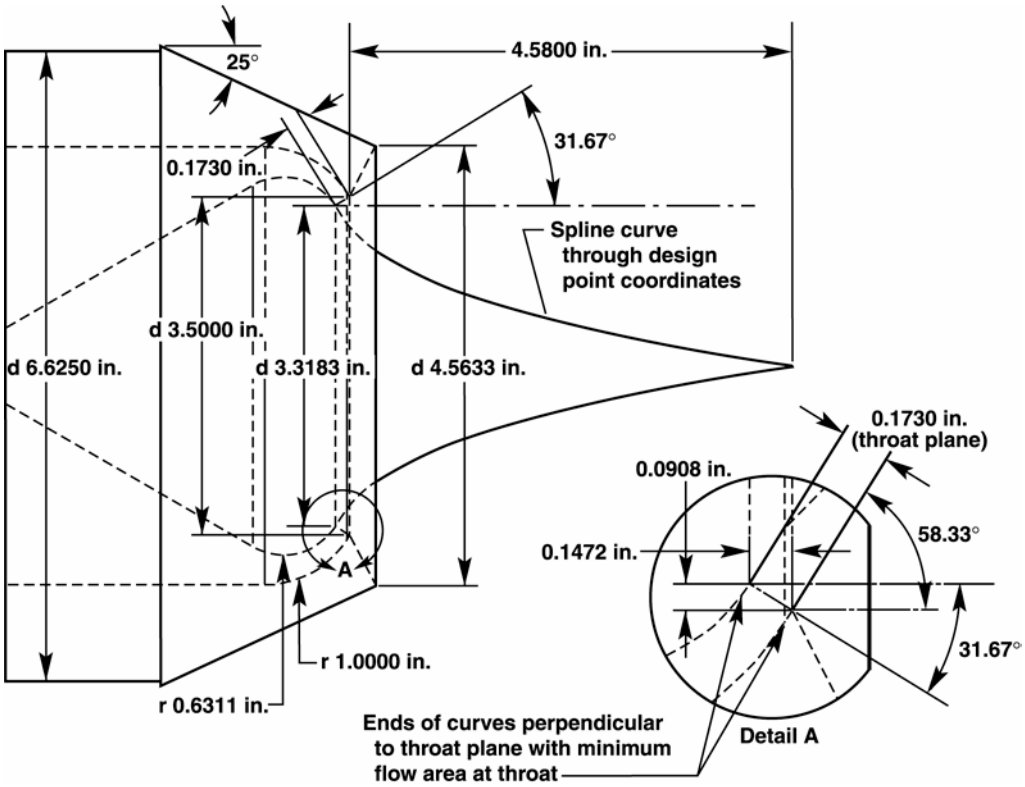

Figure 4. Aerospike Nozzle Design Flowpath for the Dryden Aerospike Rocket Test.

Axisymmetric inviscid computational fluid dynamics (CFD) analysis of the aerospike nozzle flow path was conducted for both sea level static ground firing as well as a hypothetical Mach 1.95 flight condition to determine the nozzle efficiency during static ground firing and flight test. The NASA Langley Research Center Vulcan CFD code[7] was used for the analysis. The nozzle exhaust flow was assumed to be frozen from the rocket chamber conditions. Figure 5 shows the CFD solution for the Mach 1.95 rocket flight condition. The wall pressures on the spike agree well with Prandtl-Meyer theory for both cases. The nozzle efficiency was found to be 0.96 for both the static ground firing and Mach 1.95 flight cases.

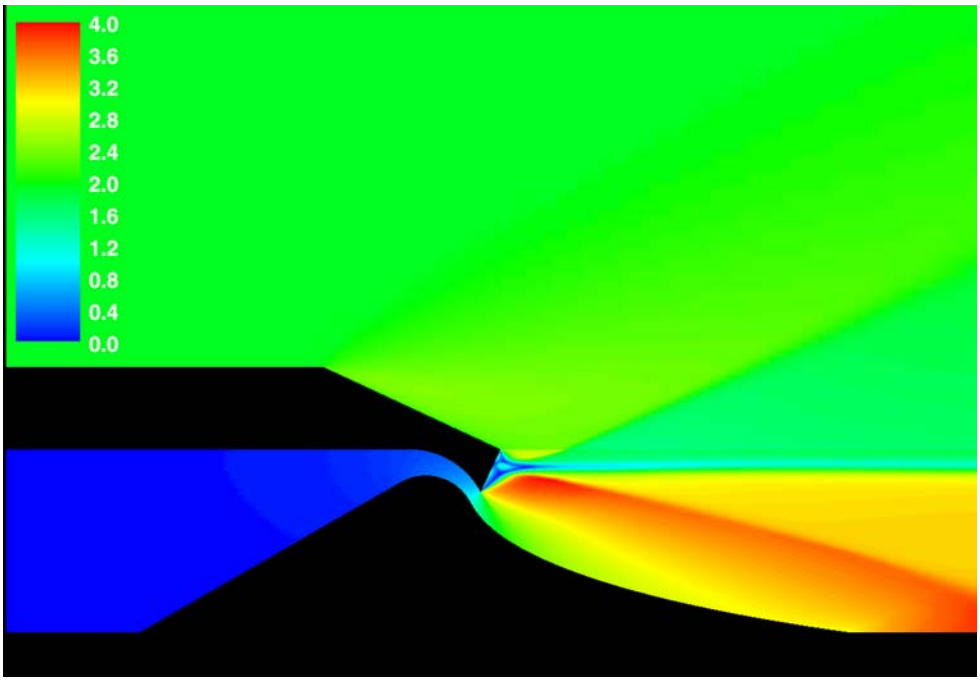

Figure 5. CFD Analysis Results for the Aerospike Rocket Nozzle at a Flight Mach Number of 1.95—Mach Contours.

Photos of the conventional conical nozzle and the aerospike nozzle are shown in figure 6. The standard conventional conical nozzle is a single piece, compression-molded phenolic with a graphite throat insert. CTI designed, developed, and fabricated the new aerospike nozzle from the flow path shown in figure 4 above. The aerospike nozzle is 2 lb heavier than the conventional conical nozzle. Both of the nozzles shown in the photos were flown as part of the flight tests.

Figure 6. Photos of the Actual CTI Conventional Conical Nozzle (Left) and Aerospike Nozzle (Right).

IV. Rocket Nozzle Ground Tests

CTI conducted four static ground firings of the motor: one with the conventional conical nozzle and three with the new aerospike nozzle. The first conventional conical nozzle and the aerospike nozzle firings were both successful. The first aerospike nozzle had minor erosion near the spike tip after firing. In an attempt to reduce the spike tip erosion, new elastomeric bonding materials were used in the second aerospike nozzle instead of the more rigid bonding materials used in the first aerospike nozzle. The new bonding materials allowed the hot gas to displace the central aerospike plug, reducing the throat area and ultimately failing a portion of the annular throat during the second aerospike nozzle firing. The more rigid bonding materials were used again in the third aerospike nozzle, and that nozzle was successfully fired. The third aerospike nozzle design was then used for both aerospike rocket flight tests.

Table 3 summarizes the ground test results. The first aerospike nozzle has similar performance to the conventional conical nozzle. This is expected, since both nozzles have the same areas and area ratios. The nozzle efficiency of the first aerospike nozzle is 0.97, in good agreement with the CFD prediction of 0.96. The third aerospike nozzle has an unreasonable nozzle efficiency value of greater than 1.0. Since 1.0 is the nozzle efficiency of an ideal, no-loss nozzle, the efficiency of a real nozzle can never exceed 1.0. In addition, the average chamber pressure and thrust of the third aerospike nozzle are significantly lower than the first aerospike nozzle and the conventional conical nozzle. The same propellant formulation was used in all of these rocket motors; therefore the lower thrust and chamber pressure in the third aerospike nozzle firing are likely to be caused by a larger actual aerospike nozzle throat area than the designed throat area. Since the designed nozzle throat area is used in the nozzle thrust coefficient calculation, a larger actual throat area would mean that the calculated nozzle thrust coefficient is too high, resulting in nozzle efficiency value greater than one.

Table 3. Results from the Rocket Nozzle Ground Tests

Ground Test	Total Impulse, lbf·s	Average Thrust, lbf	ISP, s	Average Chamber Pressure, psia	$C_{T,\ actual}$	$C_{T,\ ideal}$	Nozzle Efficiency
Conventional	6078	896.4	213.1	350.4	1.381	1.437	0.96
Aerospike 1	5866	812.0	205.6	316.2	1.386	1.426	0.97
Aerospike 3	5827	737.6	204.2	278.6	1.429	1.406	1.02

Figure 7 plots the rocket nozzle efficiency factor as a function of rocket motor burn time for all three ground tests. Motor transients during ignition and burnout cause large oscillations in the nozzle efficiency factor near t = 0 s and t = 7 seconds. The nozzle efficiency factors for the conventional and the first aerospike nozzles agree well. On the other hand, the nozzle efficiency for the third aerospike nozzle is significantly higher than the other two nozzles. As discussed in the above paragraph, this discrepancy is likely to be the result of a larger actual aerospike throat area than the designed throat area. The larger actual aerospike throat area could be caused by erosion in the aerospike nozzle throat area, expansion of the aerospike cowl structure under loads during motor firing, or unintentional throat dimensional change when the new aerospike nozzle was assembled.

Minimizing the erosion rates inside the aerospike nozzle was an important goal from the start of this effort. The solid rocket propellant was formulated with low metal loading to minimize nozzle erosion rates. Also CTI has had extensive experience with the particular grade of graphite used in both the conventional conical nozzle and the aerospike nozzle. Together with the low-metal composition of the propellant, low erosion rates inside the nozzle were expected. The ground test aerospike nozzle numbers 1 and 3 were carefully measured both before and after the ground test firings. No measurable change in dimensions was detected in the throat area for both the central spike plug as well as the external aerospike cowl. The external aerospike cowl lip remained sharp, indicating little or no erosion.

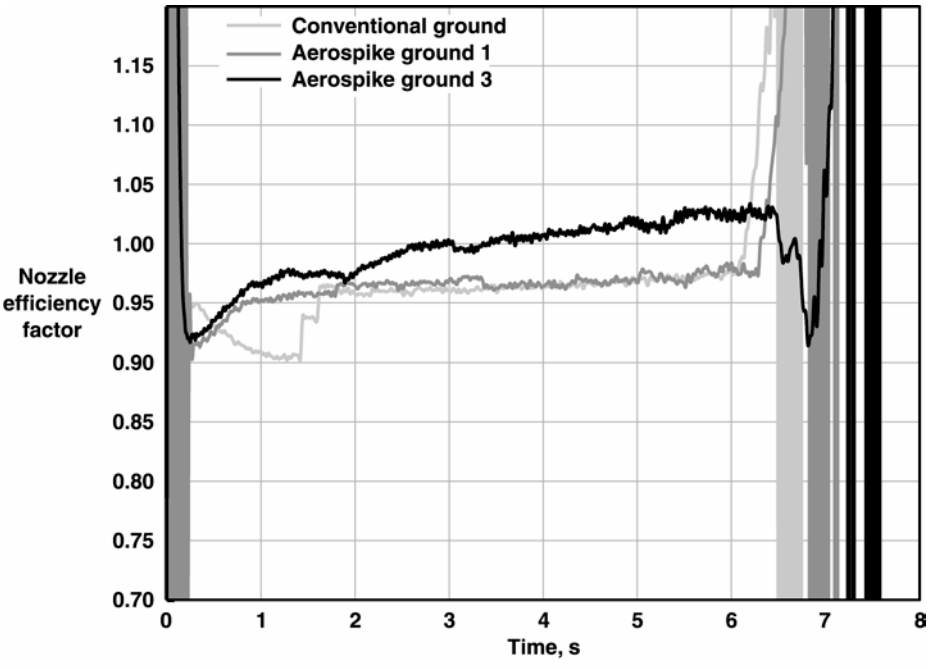

Figure 7. Nozzle Efficiency Time Histories for Three Ground Test Firings.

Other than erosion, the throat area of the aerospike nozzle can also be enlarged by expansion of the external aerospike cowl structure during motor firing. The pressure and thermal stresses from the rocket motor operation might have caused the external cowl to expand. The expansion under loads would be difficult to detect, since this expansion would only occur during motor firing. It is recommended that in future research aerospike nozzles be instrumented to monitor nozzle dimensional changes during motor firing.

Unlike the throat of the conventional conical nozzle, the current aerospike nozzle has a large-radius annulus throat around the outside of the spike plug that could be highly sensitive to dimensional variations in the tolerances in the nozzle parts as well as to the aerospike nozzle assembly procedure. Considerable care was exercised during the assembly of the current aerospike nozzles. However, specialized tooling, fixtures, or both of these might be required for an increased level of assembly precision of aerospike nozzles. A study on the effects of nozzle parts and assembly tolerances on the aerospike nozzle throat area is recommended to determine a level of required precision.

V. Rocket Nozzle Flight Tests

The blacksky Corporation conducted three rocket launches for the Dryden Aerospike Rocket Test Project: two aerospike rocket launches and one conventional rocket launch. Two aerospike rockets were flown successfully on two consecutive flights March 30 and 31, 2004 from the King Ranch Launch Site at the Pecos County Aerospace Development Corporation Flight Test Range in Fort Stockton, Texas. These rockets provided the first known set of transonic flight performance data for aerospike rockets. A planned conventional rocket launch during this launch campaign was postponed because there was more cloud cover than permitted under the flight rules. The conventional rocket launch was successfully conducted on May 18, 2005, providing baseline data for comparison with the earlier aerospike rocket flights.

Figure 8 is a photo of the final checkout of the rocket flight data acquisition system immediately before launch. After the rocket was mounted on the blacksky launch rail, the rocket flight data acquisition system was connected to a laptop PC via a high-speed serial cable, and the outputs of the entire sensor suite were monitored in real time on the laptop display to verify the sensors operation. A close-up photo of the aerospike rocket nozzle installed in the rocket on the launch rail is shown in figure 9. The launch picture of the first aerospike rocket is shown in figure 10. Both of the aerospike rockets ascended straight and true after motor ignition under calm winds and perfect skies. Both aerospike rockets were observed to be significantly louder upon takeoff than the conventional rocket using the same rocket motor. Since the aerospike nozzle uses a centered Prandtl-Meyer all-external expansion design, the

project team decided at the launch site to dedicate the second aerospike rocket flight in memory of Ludwig Prandtl and his Ph.D. student at Göttingen University, Theodor Meyer, whose work on expansion and oblique shock waves provided the theoretical foundation for the present aerospike nozzles.

Figure 8. Final Preflight Checks on the Aerospike Rocket Flight Data Acquisition System. (From left to right: Chuck Rogers, Trong Bui, and Scott Bartel.)

Figure 9. Close-Up Photo of the Aerospike Nozzle Installed in the Rocket on Launch Rail.

Figure 10. The First Aerospike Rocket Launch of the Dryden Aerospike Rocket Test.

Reference 8 provides a detailed description of the aerospike rocket launch operations. All three of the rocket launches were conducted as scheduled without major problems. The range layout and the rocket landing locations are shown in figure 11. The secured boundary of the rocket launch range for the present effort is marked by the blue pentagon that is just south of the Interstate 10 Freeway. The three predicted rocket splash patterns using a 6-degree-of-freedom trajectory analysis code with an averaged wind profile at Pecos County, Texas are also included in figure 11. The light-blue splash pattern directly below the King Ranch Launch Control site is for the no-chute case. There is no parachute deployment in this case, and the rocket continues the ballistic trajectory all the way to impact. The light-pink splash pattern in the middle is for the drogue-chute-only case where the rocket descends under drogue chute only all the way to the ground. Finally, the green pattern on the far right is for the main-chute-only case where the main chute of the rocket is deployed at apogee. Associated with each splash pattern are three concentric ovals. The smallest oval in the middle of the splash pattern is the 1-sigma (one standard deviation) boundary. The medium oval is the 3-sigma boundary, enclosing most of the splash pattern, and the largest oval is the 6-sigma boundary, encompassing the outliers. The prevailing wind pattern at high altitudes comes from the southwest direction. So when parachutes are used, the rocket drifts towards the northeast. The farthest drift occurs when the rocket descends under main chute only from apogee to the ground. Even in this worst-case scenario, the splash pattern for the rocket landing sites is fully contained within the secured boundary of the rocket launch range.

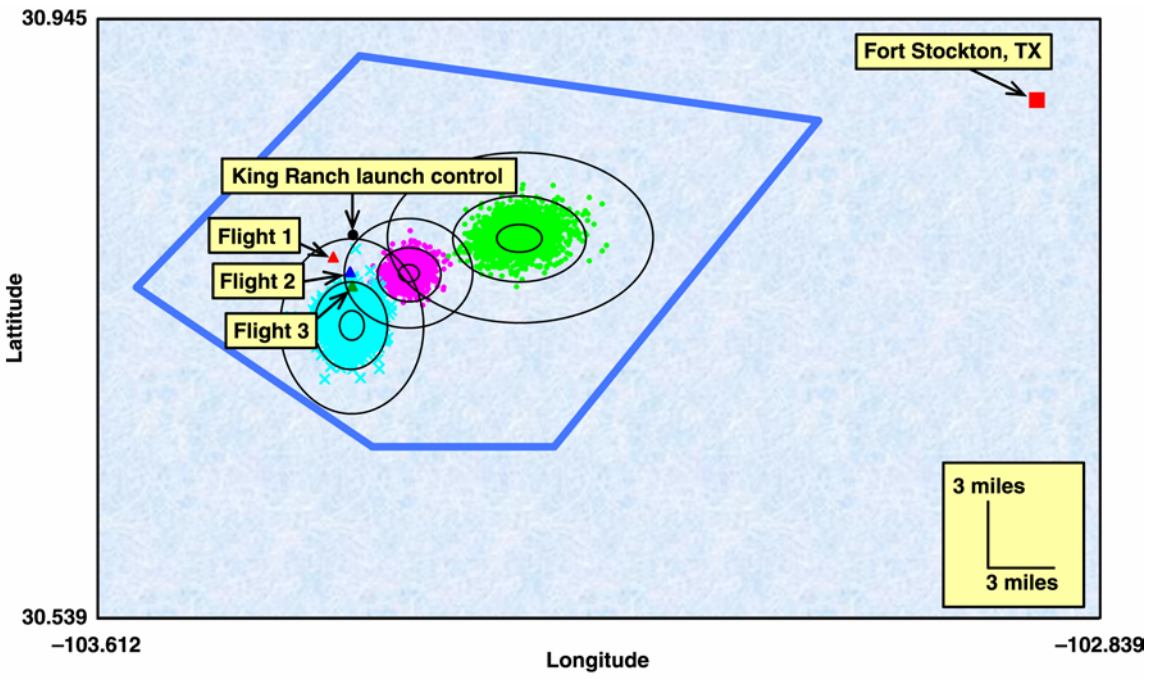

Figure 11. Rocket Range Layout and Landing Locations for the Dryden Aerospike Rocket Test.

The landing and recovery sites for rocket flights 1, 2, and 3 are 1.1 miles, 1.6 miles, and 2.2 miles, respectively, from the rocket launch site. The launch site is 2000 ft from the King Ranch launch control site. Even though the aerospike rocket flight number 1 descended under the main chute only, it landed with minimal drift because there was little or no wind on the date of launch. Aerospike rocket flight number 2 descended under the drogue chute only. However it landed a little farther from the launch site than flight 1. Finally, the conventional rocket (flight 3) flew highest. As a result, it drifted a little farther than rocket flight number 2. With the aid of the dual-redundant, onboard radio homing beacon transmitters, all of the rockets were found without major problems.

The freestream static pressure measurement on the side of the rocket airframe (corrected for position error) and the total pressure measurement at the rocket cone tip were used to compute the pressure altitude and the incoming freestream Mach number. The rocket pressure altitudes are plotted in figure 12 for the three rocket flights. The transients in altitudes at apogee are caused by the deployment of the recovery system in which the rocket nose cone is jettisoned. The apogee of the conventional rocket is about 2500 ft higher than the aerospike rockets. Aerospike rocket flight number 1 descended with deployment of the main chute only, and aerospike rocket flight number 2 descended with deployment of the drogue chute only. Both of these anomalies were caused by excessive slack in the main chute retaining line. During the first flight, the excessive slack allowed the main chute to exit the rocket airframe and deployed as soon as the drogue chute was deployed. The main chute retaining line was shortened for the second aerospike flight. However, there was still enough slack in the retaining line to tangle the main chute bag, preventing it from deploying, and the rocket descended on the drogue chute only. This problem was corrected for the conventional rocket launch in the following year, and the conventional rocket descended under both the drogue and main chutes as designed. However, as can be seen in figure 12, the main chute deployed at only approximately 500 ft above ground level instead of 2500 ft as planned. Since 500 ft above ground level is the default main chute deployment altitude setting for the blacksky AltAcc units, it is likely that these units were not programmed for the planned main chute deployment altitude prior to flight. All of these recovery modes were anticipated before the rocket launches, the rocket launch range was planned to accommodate all possible chute combinations, and mission success was achieved in all cases. From altitude as compared with time plots in figure 12, the drag coefficients of the drogue and main chutes were calculated to be 0.59 and 0.88, respectively. The average rocket descent velocities were 61.8 mph using the drogue chute and 21.3 mph using the main chute.

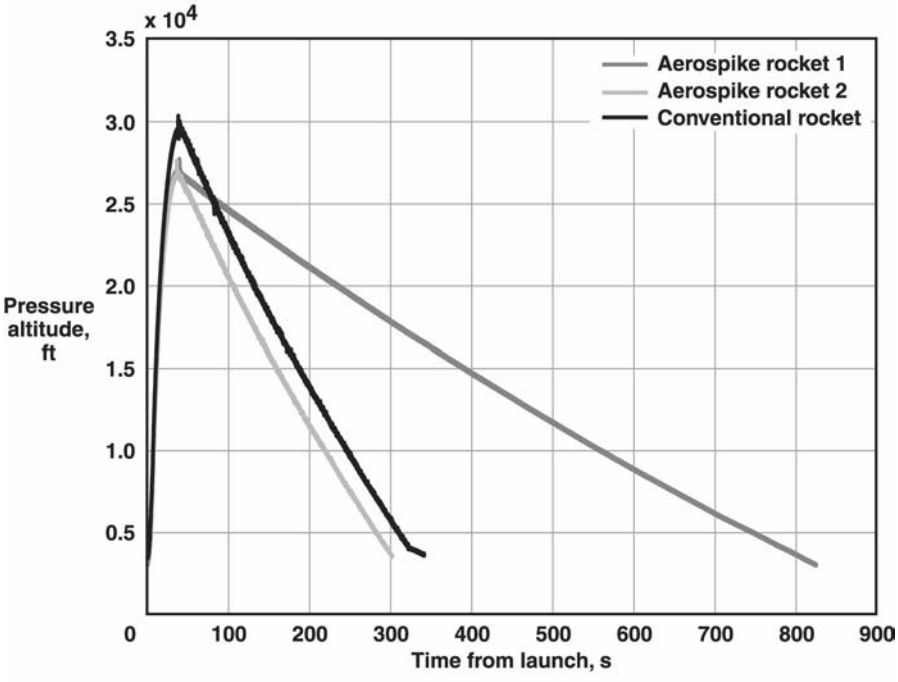

Figure 12. Pressure Altitudes for Three Rocket Flights.

Rocket flight Mach numbers plotted in figure 13 show that the conventional rocket attained the highest maximum Mach number, approximately 1.6. Both aerospike rockets reached a lower maximum Mach number of approximately 1.5. As the rockets decelerate and reach apogee, there is more noise in the flight Mach number calculated from the rocket pitot-static system. The onboard axial accelerometer recorded a maximum of 12.5 *g* and a minimum of –4 *g* for flight number 1, 12.0 *g* to –3.9 *g* for flight number 2, and 13.4 *g* to –3.8 *g* for flight number 3. The altitude, Mach number, and acceleration flight results indicate that the conventional rocket performed better than the aerospike rockets. Also, aerospike rocket flight number 1 performed marginally better than aerospike rocket flight number 2.

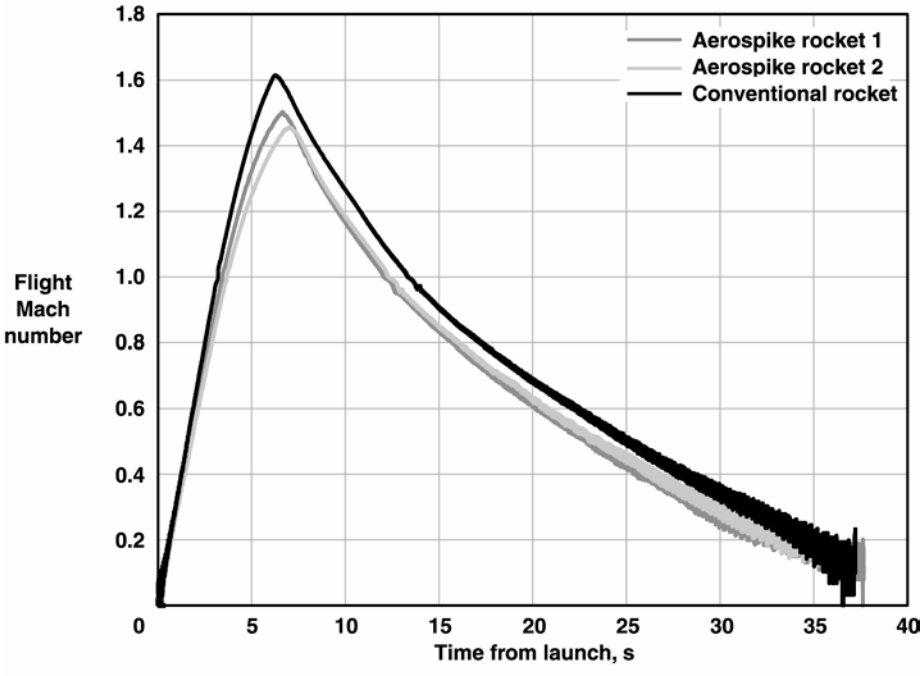

Figure 13. Flight Mach Numbers for Three Rocket Launches.

The conventional rocket was 2 lb lighter than the aerospike rockets because of the heavier aerospike nozzle hardware. But one major reason for the higher performance of the conventional rocket may be found in figure 14. When the rocket motor is off, it is possible to compute the rocket drag in flight using equation (7) by setting the rocket thrust to zero. The conventional rocket has significantly lower drag than either of the aerospike rockets, both subsonically and supersonically. This is surprising, since the aerospike rocket with a long spike at the base, would have been expected to have lower base drag than the conventional rocket, which is basically blunt at its base. All three rockets exhibit an unexplained second peak in the drag curve in the range of Mach 1.3 to 1.5. The conventional rocket also has a smaller second peak.

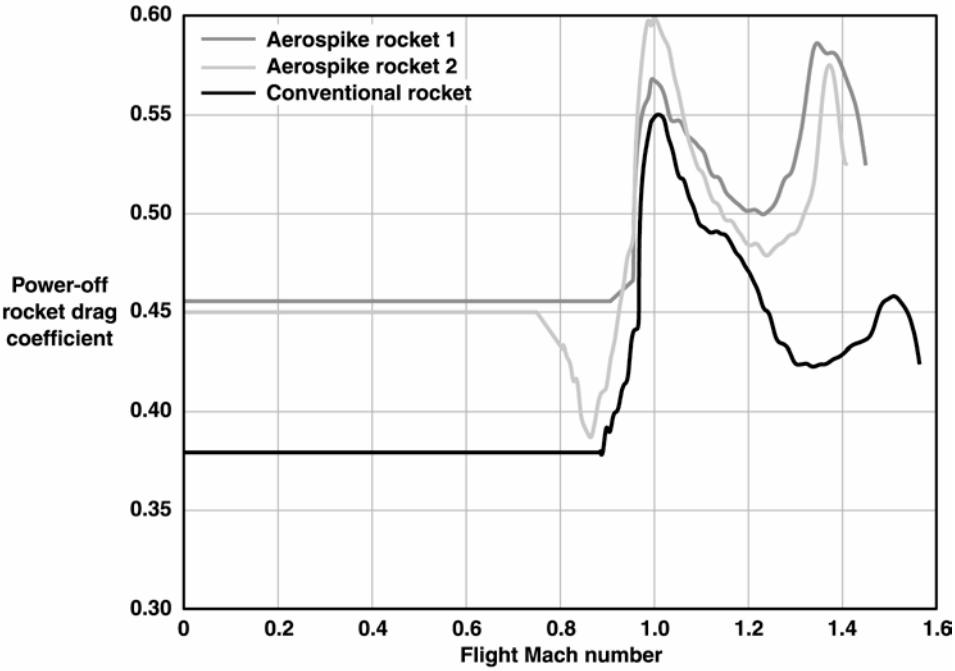

Figure 14. Power-Off Drag Coefficient for Three Rockets.

The increased flight performance of the conventional rocket is also a result of the increased conventional rocket motor performance, as summarized in table 4 below. The conventional rocket motor has the highest total impulse, average thrust, and average chamber pressure. The in-flight performance of the conventional rocket motor agrees well with the conventional rocket ground test firing. The aerospike rocket flight number 1 has higher total impulse, average thrust, and ISP than the aerospike rocket flight number 2. The nozzle efficiency of the conventional conical nozzle seems reasonable, though lower than its efficiency during static ground firing. The aerospike nozzle flight number 2 also has an unreasonable efficiency value of greater than one, similar to the aerospike nozzle ground test number 3.

Table 4. Results from the Rocket Nozzle Flight Tests

Flight Test	Total Impulse, lbf·s	Average Thrust, lbf	ISP, s	Average Chamber Pressure, psia	$C_{T,\ actual}$	$C_{T,\ ideal}$	Nozzle Efficiency
Conventional	6240	898.5	218.7	349.4	1.388	1.475	0.94
Aerospike 1	6224	856.1	218.2	N/A	N/A	N/A	N/A
Aerospike 2	6089	790.8	213.4	278.6	1.532	1.435	1.07

The decreased aerospike rocket thrust and total impulse are a result of lower rocket chamber pressures. Figure 15 plots the measured rocket chamber pressures for the rocket static ground firings as well as flight tests. All of the measured rocket chamber pressures follow a similar shape. In general, increased rocket chamber pressures result in shorter burn times. The chamber pressures for conventional motors are consistently higher than aerospike motors. As discussed in the "Rocket Nozzle Ground Tests" section above, this is most likely caused by a larger actual aerospike nozzle throat area than the designed throat area. For a solid propellant rocket motor, an increase in the nozzle throat area would cause a corresponding decrease in chamber pressure and a longer burn time, as shown in the measured chamber pressure data in figure 15. Also note that the chamber pressures of the aerospike nozzles have a constant offset from those of the conventional conical nozzle. If the aerospike nozzles were to be eroding at a higher rate than the conventional conical nozzles, one would expect to see a more regressive or a different profile altogether, given similar ballistic properties in all the motors. Visual examination of the postflight aerospike nozzles reveal extensive cracks throughout the external cowl as well as on the spike plug, caused by the ablative core continuing to pyrolize and expand from the residual heat in the graphite after the motor shuts down. Also, there were impact damages to the aerospike nozzles resulting from the landings on rocky grounds. The external aerospike cowl lips remained sharp with little evidence of erosion.

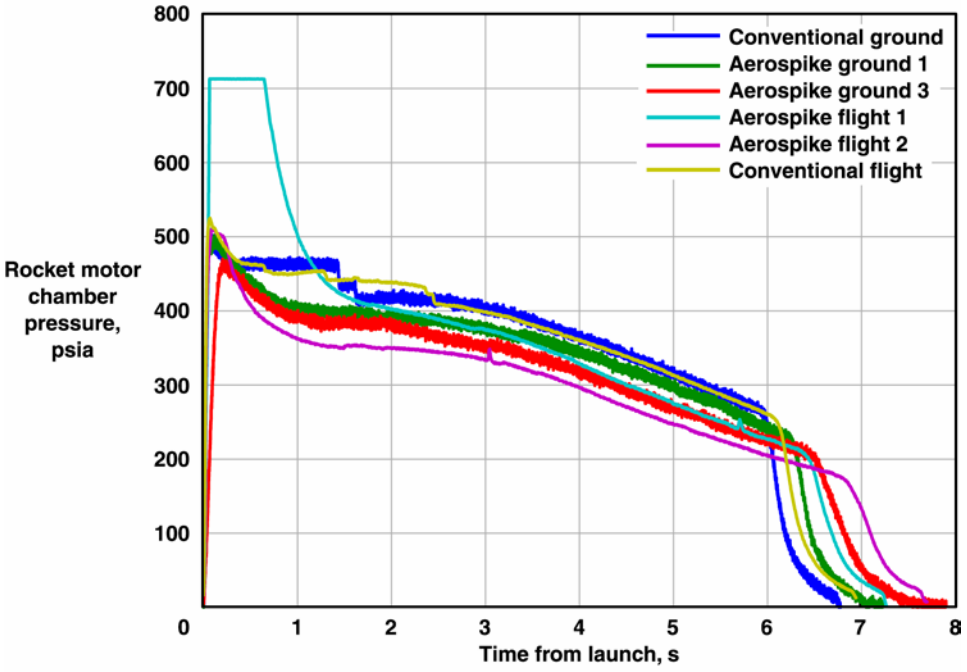

Figure 15. Measured Rocket Chamber Pressure for Ground and Flight Tests.

During the aerospike rocket flight number 1, the hot rocket chamber gas was allowed to impinge directly upon the sensing diaphragm of the rocket chamber pressure transducer. Even though the stainless steel chamber pressure transducer was designed to operate in hostile environments, the direct impingement of the hot gas on the sensing diaphragm caused the transducer to produce erroneous pressure measurements for approximately the first two seconds of rocket motor firing because of the transient thermal inequilibrium that resulted at the sensing diaphragm. This phenomenon can be seen in an abnormal peak during the first two seconds of the aerospike flight number 1 data. Data after the first two seconds seem reasonable once the pressure transducer is uniformly hot. In the subsequent aerospike rocket flight number 2, as well as the conventional rocket flight, silicon vacuum grease was used to pack the pressure transducer port. This shielded the pressure sensing port from the direct impingement of hot rocket gas, and good chamber pressure measurements were obtained for these later flights.

The rocket motor thrusts for all conventional and aerospike motors, both on the ground and in flight, are compared in figure 16. The conventional motor thrust curves are consistently higher than the aerospike motor thrust curves, both on the ground and in flight. The lower aerospike motor thrust levels are most likely caused by the larger aerospike nozzle throat area, reducing rocket chamber pressure, as discussed above. It is interesting to note that the

conventional rockets consistently hold higher chamber pressure and thrust than the aerospike rockets immediately after ignition; and the aerospike rockets lack the discontinuous vertical steps in chamber pressure and thrust that are seen in the conventional rockets. The discontinuous steps in chamber pressure and thrust seen in the conventional rockets occur occasionally in other solid rocket motors as well. The steps show up in both of the conventional rocket motor firings, in flight as well as on the ground. But none is present in any of the aerospike rocket firings. Note that the ground test data in both figure 15 and 16 are noisier than the flight test data. This is simply caused by a higher data sampling rate during the ground tests (1000 Hz).

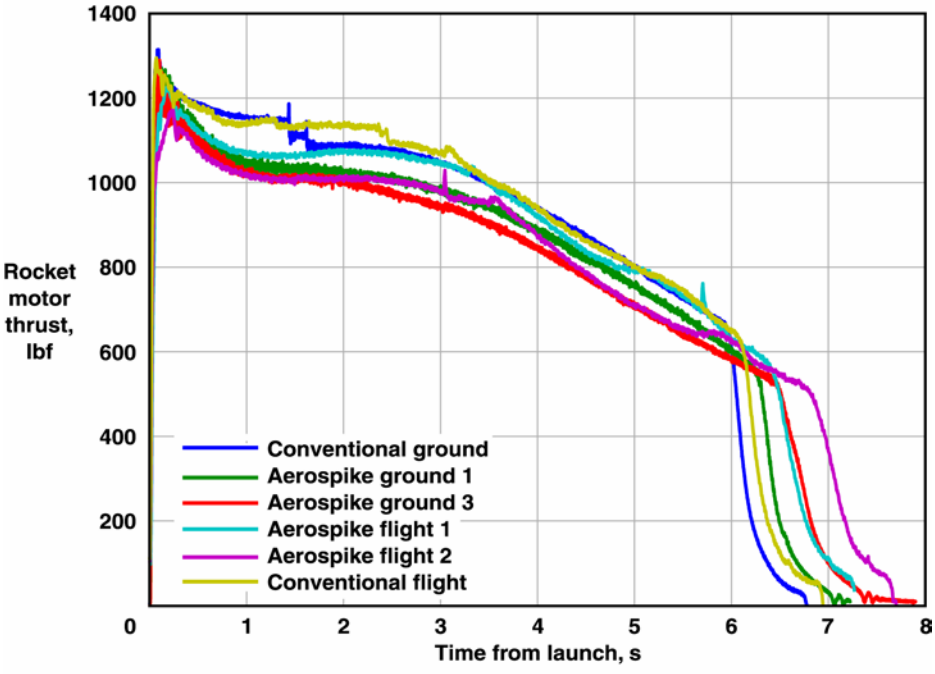

Figure 16. Rocket Motor Thrust Curves for Ground and Flight Tests.

VI. Conclusions

Flight research of an aerospike rocket nozzle was conducted using high power solid rockets. Two aerospike rockets and one conventional rocket were flown successfully to supersonic speeds, providing the first known set of transonic flight performance data for aerospike rockets. Even though the aerospike rockets flew well, the chamber pressures and thrusts of the aerospike rocket motors were lower than the conventional rocket motors, both in the static ground firings and flight tests. Since the same propellant formulation was used in all of the motor grains, the lower aerospike chamber pressures and thrusts were likely to be caused by a larger actual aerospike nozzle throat area than the designed throat area. The larger actual aerospike throat area was also potentially the cause of the computed aerospike nozzle efficiencies being greater than 1.0 in some of the tests. The larger throat area might have been caused by erosion in the aerospike nozzle throat area, expansion of the aerospike external cowl structure under loads during motor firing, or unintentional throat dimensional change caused by tolerances in nozzle parts or by assembly procedure. While efforts were made during this project to minimize the aerospike nozzle erosion rates, more attention should be given to the potential problems of aerospike cowl expansion under loads and unintentional throat dimensional change. The power-off, in-flight drag of the aerospike rockets was found to be higher than the conventional rocket. As a result, the integration of the aerospike nozzle assembly to the rocket base should be examined more carefully in future efforts. Finally, the aerospike rockets were observed to be significantly louder at launch than the conventional rocket.

The national space exploration goals would benefit greatly from rapid progress in the development of advanced aerospace technologies. A closer connection amongst analysis, ground testing, and flight testing activities than ever before is required to achieve this progress. New and advanced aerospace technologies must be taken to flight early to "… separate the real from the imagined, and to make known the overlooked and the unexpected problems…" as Hugh Dryden once said.

The rocket vehicle, flight operation procedures, and the rocket flight data acquisition system were found to perform well, and these would form an excellent, cost-effective foundation for future follow-on efforts in high-speed flight research for aerospike nozzles as well as other advanced space vehicle technologies. As a result of the present study, the following recommendations are suggested for future work:

1. Investigate and correct aerospike nozzle problem(s) that caused the lower aerospike rocket chamber pressure and rocket thrust, as well as the unreasonably high aerospike nozzle efficiencies.
2. Measure or compute the difference between power-on and power-off drag coefficients for rockets of this configuration. Determine the cause for the higher power-off drag found in the aerospike rocket.
3. Conduct flight research on spike truncation effects on aerospike nozzle performance in flight using small rockets. Compare the performance to a full-length aerospike nozzle in flight.
4. Conduct flight research on altitude compensation of aerospike nozzles at a wider range of altitudes as well as in space using large high power rockets or small sounding rockets. Compare the performance to bell or conical nozzles.
5. Conduct flight research on two-phase flow effects from high metal content in solid rocket propellant on aerospike nozzle performance using small rockets.
6. Conduct flight research on altitude compensation of dual bell nozzles using small rockets. Compare the performance to aerospike nozzles and bell nozzles.
7. Conduct flight research on the effects of altitude-compensating nozzles on the performance of air-to-air, ground-to-air, or ground-to-ground missile weapon systems for defense applications.

References

[1]Gerald Hagemann, Hans Immich, Thong Van Nguyen, and Gennady E. Dumnov, "Advanced Rocket Nozzles," Journal of Propulsion and Power, Vol. 14, No. 5, 1998, pp. 620-634.

[2]J. H. Ruf and P. K. McConnaughey, "The Plume Physics Behind Aerospike Nozzle Altitude Compensation and Slipstream Effect," AIAA Paper 1997-3218, 1997.

[3]R. T. Johnson, Jr. and B. A. Leary, "An Aerospike Nozzle Design for Solid Aluminized Composite Rocket Propellant," 20th JANNAF Rocket Nozzle Technology Subcommittee Meeting, CPIA Publication 694, CPIA, Columbia, MD, November 1999, pp. 103-111.

[4]Eric Besnard, Hsun Hu Chen, Tom Mueller, and John Garvey, "Design, Manufacturing and Test of a Plug Nozzle Rocket Engine," AIAA Paper 2002-4038, 2002.

[5]Stephen A. Whitmore and Timothy R. Moes, "The Effects of Pressure Sensor Acoustics on Airdata Derived From a High-Angle-of-Attack Flush Airdata Sensing (HI-FADS) System," NASA TM 101736, 1991.

[6]Che-Ching Lee, and Donald D. Thompson, "FORTRAN Program for Plug Nozzle Design," NASA TM X-53019, 1964.

[7]J.A. White and J.H. Morrison, "A Pseudo-Temporal Multi-Grid Relaxation Scheme for Solving the Parabolized Navier-Stokes Equations," AIAA Paper 99-3360, 1999.

[8]Scott Bartel and Charles E. Rogers, "The Dryden Aerospike Rocket Test (DART) Project – Launch Report for Aerospike Rocket Flights," High Power Rocketry, Vol. 35, No. 5, August 2004, Published by Tripoli Rocketry Association. pp. 6-46.